NACA RM E54F14

NACA

RESEARCH MEMORANDUM

EXPERIMENTAL DETERMINATION OF AERODYNAMIC FORCES NORMAL TO THE CHORD DUE TO ROTATING STALL ACTING ON COMPRESSOR BLADING

By Donald F. Johnson and Eleanor L. Costilow

Lewis Flight Propulsion Laboratory
Cleveland, Ohio

NATIONAL ADVISORY COMMITTEE
FOR AERONAUTICS

August 24, 1954
Declassified June 20, 1957

NATIONAL ADVISORY COMMITTEE FOR AERONAUTICS

RESEARCH MEMORANDUM

EXPERIMENTAL DETERMINATION OF AERODYNAMIC FORCES NORMAL TO THE CHORD DUE TO ROTATING STALL ACTING ON COMPRESSOR BLADING

By Donald F. Johnson and Eleanor L. Costilow

SUMMARY

An investigation was conducted on an NACA axial-flow single-stage compressor having a 14-inch diameter and a 0.9 hub-tip ratio to determine the magnitude of the blade force variation due to the flow fluctuations caused by rotating stall. The blade forces were determined from calibrated wire-resistance strain gages and the flow fluctuations determined by means of hot-wire anemometers. These results were obtained pertaining to the aerodynamic forces normal to the blade chords of the stators and inlet guide vanes caused by rotating stall in the compressor.

At the guide vane inlet the maximum flow between stall zones was 1.3 of the average flow rate and the minimum flow rate in the stall zone was 0.08 of the average flow rate. The frequency with which the stall zones passed the guide vanes and stators was 51 cps.

The amplitude of the force variation on the stators was equal to the maximum steady-state force on the stators. The amplitude of the oscillatory force on the guide vanes was two to three times the steady-state force at the maximum flow rate between stall zones.

INTRODUCTION

Rotating stall has recently come into prominence as a possible source of excitation for compressor blade vibration (ref. 1). Reported investigations have been primarily concerned with the determination of the number of stall zones formed in the compressor annulus, their propagation rate (refs. 2 and 3), and their role in exciting compressor blades to vibrate. Reference 4 shows that large stresses can be produced in compressor blades which are excited to resonance by rotating stall. The vibratory stress at resonance depends, however, on the blade damping and the strength of the excitation force. The strength of the excitation forces due to rotating stall has not been investigated.

Reference 5 discusses several factors that affect blade damping. The author of reference 6 suggests that the flow rate between stall zones may be sufficiently low to cause stall flutter; that is, the aerodynamic damping may be negative.

The purpose of this investigation was to determine by means of suitably mounted wire resistance strain gages the time variation of the aerodynamic force normal to the blade chord (axis of minimum cross-sectional moment of inertia) when rotating stall exists. In addition, it was desired to measure the steady-state forces on the blading during unstalled operation and, if possible, to correlate the blade forces measured under stalled conditions with the steady-state forces.

APPARATUS AND INSTRUMENTATION

Compressor

The single-stage compressor used in this investigation was an NACA axial-flow compressor having a 14-inch diameter and a 0.9 hub-tip ratio, and consisting of 38 steel inlet guide vanes, 31 aluminum rotor blades, and 32 cantilevered aluminum stator blades. The blades were untwisted, untapered, and designed for a symmetrical velocity diagram at the pitch radius as shown in figure 1. NACA 65(12)-10 blower blade profiles were used for both the rotor and stator at all radii. The guide vanes were circular-arc sheet-metal vanes.

A schematic diagram of the compressor test setup is shown in figure 2. Air entered through the orifice tank and a motor-driven inlet throttle into a depression tank where screens were used to straighten the air at the compressor inlet. The compressor air discharged into a receiver and then through an outlet throttle to the altitude exhaust system.

Instrumentation for Flow Measurements

The rotating-stall characteristics of the compressor were determined by the use of constant-temperature hot-wire anemometers made of 0.0002-inch-diameter tungsten wire with an effective length of 0.08 inch. The wire element was mounted perpendicular to the axis of the probe and oriented normal to the mean air-flow direction at approximately midspan of the blade. The amplifier used in conjunction with the hot-wire probes was that reported in reference 7.

The output of the hot-wire anemometer was viewed on a cathode-ray oscilloscope and the flow fluctuations were recorded photographically.

Instrumentation for Blade Force Measurements

Four inlet guide vanes and four stator blades were modified and mounted as shown in figure 3 to accommodate resistance-wire strain gages. In order to provide adequate strain-gage sensitivity as well as a range of blade natural frequencies, it was necessary to reduce the blade shanks to web sections of various thicknesses ranging from 1/16 inch to 1/8 inch. The experimentally determined natural frequencies of the blades are given in table I.

Two strain gages were mounted side by side on each face of the web section of the shank of every blade. The four gages on each blade were wired in a bridge circuit consisting of four active legs. Each bridge was powered by a battery power supply and its output was amplified by a high-gain d-c amplifier. The amplified outputs were recorded from the screen of a four-channel cathode-ray oscilloscope. The strain-gage outputs from four blades could be observed or recorded simultaneously if necessary.

CB-1 back

Each instrumented blade was calibrated statically by hanging weights at the midspan position of its blade section and noting resultant beam deflection on the oscilloscope.

The aerodynamic forces imposed upon the blades as they encountered a stall zone were measured by the oscilloscope in conjunction with a low-pass electronic filter that was set to attenuate the components of the strain-gage deflection signal above 250 cps or approximately five times the stall frequency. The rate of attenuation in the rejection band of the filter, that is, frequencies greater than 250 cps, is 18 decibels per octave. In order to assure restoration of the blade to the static load position (to prevent overlapping of transient vibration) between successive impulses by the stall zone, it was found necessary to incorporate additional viscous damping. The damping required was obtained by packing a light grease around the blade shank as indicated in figure 3. A discussion of the use of the rejection filter and grease is contained in appendix B.

PROCEDURE

In a typical run, flow measurement data were taken with hot-wire probes located at stations 0 and 3 as indicated in figure 2. The frequency of the rotating stall was determined by forming Lissajous figures on the oscilloscope by use of an audiofrequency oscillator. Reference 2 describes the methods used in determining the number of stalls and the method by which the amplitude of the flow fluctuations was determined from the anemometer output.

In general, quantitative blade force runs were made with one blade at a time observed on the oscilloscope. The position of the beam on the oscilloscope was noted before the compressor was started. For various weight flows (compressor unstalled) at a compressor speed $N/\sqrt{\theta}$ of 167 rps the deflection of the oscilloscope beam was recorded in order to determine the magnitude of the blade force during unstalled operation. Next the compressor was stalled and the amplitude of the oscilloscope beam deflection recorded giving the blade force variation during compressor-stall operation. At first, data were taken with no damping but all later data were taken with the blades damped as mentioned in the previous section and explained more fully in appendix B.

RESULTS AND DISCUSSION

Experimentally determined steady-state blade forces, that is, those forces existing during unstalled compressor operation, are shown in figure 4. The steady-state forces were estimated in order to indicate trends that might be expected in the experimental data. The calculations were made by the method of reference 8, where boundary layers, secondary flows, tip-clearance effects, and so forth are neglected. The results of such a calculation, shown in figure 4, consider $22\frac{1}{2}^{\circ}$ turning in the guide vanes and a relative discharge angle for both the stators and guide vanes of $22\frac{1}{2}^{\circ}$. The change in discharge angle with angle of attack in the stator and rotor was ignored.

The general shapes of the calculated and experimental steady-state force curves shown in figure 4 correspond for both the guide vanes and stators. The lack of quantitative agreement between experimental and calculated force values for the stators can in part be attributed to several factors that have been neglected in the calculated force value which would tend to reduce these values. It is known that since the blade height is small for this stage the boundary-layer losses which are not accounted for will be appreciable. In addition, no diffuser efficiencies have been applied to the calculated stator forces which would result in a reduction of the calculated force value. Also, the method employed here has assumed a concentrated force at the mean blade height, whereas the experimental data represent the actual force as distributed over the entire blade span. The aggregate result of these factors would be a reduction of the calculated blade force so that the values determined by the method of reference 8 do not seem unreasonably high. One reason for the spread in experimental data is the drift in the d-c amplifier, which may account for an error of ± 10 percent in the measurement of such small forces. The development of the equations for calculating the steady-state blade forces is given in appendix C.

Figure 4 shows that the calculated steady-state blade force for the guide vanes increases with weight flow. The experimental data exhibit this same characteristic trend and show reasonable agreement quantitatively. The calculated steady-state blade force on the stator increases up to a weight flow of 4.5 pounds per second, after which it decreases slowly. Because the compressor stalled at a weight flow of 3.45 pounds per second, the calculated force on the stator for lower weight flows was terminated since the flow direction does not conform to those of the velocity diagram. The experimental values for the steady-state force on the stators show a rapid increase for weight flows above the stall limit and a rapid falling off at about 4.5 pounds per second. Quantitative agreement was not achieved for the reasons discussed earlier.

The compressor was operated at the stalled condition, where the oscillatory blade forces were measured. The operating point is indicated by point A on the compressor performance map given in figure 5. A typical oscillogram of the hot-wire output for this operating point is shown in figure 6; the trace is from the hot-wire anemometer at station 0 about 1/2 inch upstream of the guide vanes. When the method of reference 2 was applied to the oscillogram given in figure 6, the annulus was found to contain one stall zone having a frequency of 51 cps. The stall zone was revolving at about 31 percent of rotor speed in the direction of rotor rotation (absolute frame of reference) and covered about one-third of the annulus area. The same stall pattern was reported for this compressor in reference 2.

The time variation in weight flow (fig. 7) was determined from the hot-wire anemometer oscillogram by the method given in reference 2. The ratio of the maximum to the mean value of the weight flow $\Delta\rho V/\overline{\rho V}$ is almost 1.3. (All symbols appearing in the text are given in appendix A.) At the low flow point in the rotating stall, the weight flow is reduced to approximately 0.26 pound per second and the maximum between stalls, 4.5 pounds per second. Since the flow rate between the stall zones is greater than that which caused stall (3.45 lb/sec) for this particular compressor, it seems unlikely that stall flutter could occur between stall zones as suggested in reference 6.

A trace of the hot-wire anemometer signal at station 3, 1/2 inch downstream of the stators, is shown in figure 8. This signal is different from that observed at station 0 in that a small rise in the center of the stall zone exists. This phenomenon is interpreted as a region of reversed flow within the stall zone.

When the compressor was stalled, the rotating stall region developed in the annulus imposed oscillatory aerodynamic forces on the compressor blading. Typical oscillograms of the strain-gage output from stators 2 and 4 (see table I) and a hot-wire anemometer at station 3 are shown

in figure 8. These records were taken without any viscous damping. The reaction of a blade without viscous damping when impinged upon by a stall zone depended upon its position in its vibration cycle and its velocity at the time of impingement. This reaction is illustrated by the difference in size between succeeding transients.

In order to eliminate the overlapping of the transients and the attendant high vibratory stresses, grease was inserted around the web and shank of the blades as shown in figure 3.

Typical oscillograms of the strain-gage output, which is proportional to blade deflection, taken with grease around the web section and shank are shown in figure 9. It can be seen that in the case of the guide vanes the grease was sufficient to damp out the transients between successive impingements upon the blades by the stall zones. However, in the case of the stators, even though the grease was sufficient to nearly eliminate the transients between stall zones, a certain amount of random blade motion remained. The transients in the stators did not exhibit the reproducibility between stall zones as did those in the guide vanes.

The damping was adequate to prevent the overlapping of the transients. However, it was not so great as to affect seriously the determination of the blade force because the natural frequencies of the blades were several times the frequency of the stall zones; hence, the magnification factors were near unity for the first five harmonics. The wave form of the force variation was observed with a progressively lower setting of the filter. Although the basic wave form may have changed, because of the phase shifts of the higher harmonics, the amplitude did not. Therefore, it was possible to filter out the transients without seriously changing the wave form of the force variation. The filtered strain-gage outputs were considered to be the wave form of the force variation caused by the impingement of the stall zone on a blade. The theory behind this use of a filter is explained in appendix B. As was mentioned in the procedure, the filter was set at low pass, 250 cps. Therefore, the fundamental of the forcing function and its first four harmonics were unattenuated and frequencies above 250 cps were attenuated at 18 decibels per octave. The attenuation of the transients depended upon the natural frequency of the blade in question. Typical filtered outputs are shown in figure 10. The amplitude of the force variation as indicated by the oscillograms showed agreement among the four instrumented blades in each of the two blade rows; that is, stators and guide vanes. Although not all of the transients were completely attenuated by the filter setting used, the wave forms presented in figure 10 are representative of the wave form of the force variation. In order to make the reported values of the amplitude of the oscillatory force nondimensional, the amplitude of the time variation in force due to rotating stall was divided by the steady-state blade force at the maximum weight flow between stall zones. The

maximum weight flow between stall zones indicated in figure 7 was 4.5 pounds per second. The corresponding steady-state blade forces for both the guide vanes and stators are indicated in figure 11, where the averaged experimental steady-state force values are given. The ratio of the amplitude of the oscillatory force to this steady-state force was found to be 2:1 to 3:1 for the guide vanes and approximately 1:1 for the stators. At present no explanation for the difference in the force ratios between the stators and guide vanes is available. No reversed flow after the guide vanes that might contribute to the higher force could be detected. The results reported were reproducible over a period of time.

SUMMARY OF RESULTS

An investigation was conducted on an NACA axial-flow single-stage compressor having a 14-inch diameter and a 0.9 hub-tip ratio to determine the magnitude of the blade force variation due to the flow fluctuation caused by rotating stall. The blade forces were determined from calibrated wire-resistance strain gages and the flow fluctuations determined by means of hot-wire anemometers. These results were obtained pertaining to the aerodynamic forces normal to the blade chords of the stators and inlet guide vanes caused by rotating stall in the compressor:

1. At the guide vane inlet the maximum flow between stall zones was 1.3 of the average flow rate and the minimum was 0.08 of the average flow rate. The frequency with which the stall zones passed the guide vanes and stators was 51 cps.

2. The amplitude of the force variation on the stators was equal to the maximum steady-state force on the stators. The amplitude of the oscillatory force on the guide vanes was two to three times the steady-state force at the maximum flow rate between stall zones.

Lewis Flight Propulsion Laboratory
National Advisory Committee for Aeronautics
Cleveland, Ohio, June 9, 1954

APPENDIX A

SYMBOLS

The following symbols are used in this report:

A	compressor annulus area, sq ft
a_k	coefficient in Fourier series representation of blade force variation
D	magnification factor
F	aerodynamic force normal to blade chord, lb
F^*	maximum value of blade force, F, during stalled operation
f_n	natural frequency of compressor blade, cps
f_s	stall frequency, cps
g	gravitational constant, 32.2 ft/sec^2
k	integer (see appendix B)
N	compressor speed, rps
n	number of blades
R	ratio of hub radius to tip radius
t	time, sec
U	blade velocity, ft/sec
V	absolute air velocity, ft/sec
W	relative air velocity, ft/sec
w	weight flow, lb/sec
X	V_u/U_t
x	blade deflection, ft
x'	blade deflection for 1 pound force normal to blade chord at midspan position, ft

Y	V_a/U_t
y	x/x'
α	blade turning angle
δ	$P_1/14.7$
ζ	damping ratio
θ	$T_1/518.6$
ρ	air density, lb/cu ft
$\frac{\Delta\rho V}{\overline{\rho V}}$	amplitude of flow fluctuation divided by ρV based on average current through hot wire
τ	time duration of blade force variation as a stall zone passes a compressor blade, sec
φ	phase shift
ω_n	undamped natural frequency of blade, rad/sec

Subscripts:

a,u	axial and tangential components, respectively
gv	guide vane
m	mean
s	stator
t	rotor tip
o	steady state
0	before guide vane
1	before rotor
2	before stator
3	after stator
p,q,r	used to indicate terms in blade response equation in appendix B
i,j	indices on phase shift term in appendix B

APPENDIX B

RESPONSE OF COMPRESSOR STATOR TO THE VARIATION IN AERODYNAMIC BLADE FORCE DUE TO ROTATING STALL

The variation in aerodynamic loading normal to the chord of a compressor blade as a stall zone passes the blade may be represented by the following expression:

$$F(t) = F^* - \sum_{k=1}^{\infty} a_k \left[\sin \frac{k\pi t}{\tau} - \cos k\pi \sin \frac{k\pi}{\tau} (t - \tau) \right] \tag{B1}$$

where F^* is the time steady blade force normal to the blade chord for flow conditions outside the stall zone and

$$F(t) = F^* \quad \text{for} \quad t \leq 0 \quad \text{and} \quad t \geq \tau \tag{B2}$$

(note: any function of $t - \tau \equiv 0$ for $t < \tau$)

The deflection of the blade from its position with the steady force F^* acting is given by the following equation:

$$\frac{d^2(y - y^*)}{dt^2} + 2\zeta\omega_n \frac{d(y - y^*)}{dt} + \omega_n(y - y^*)$$

$$= -\omega_n^2 \sum_{k=1}^{\infty} a_k \left[\sin \frac{k\pi}{\tau} t - \cos k\pi \sin \frac{k\pi}{\tau} (t - \tau) \right] \tag{B3}$$

where y^* is the blade deflection due to force, F^*.

In general, with operation in rotating stall, the blade will not be stationary when it encounters a stall zone but will be vibrating from the effects of the previous encounter with a stall zone. Then the initial conditions may be stated as follows

$$\left.\begin{aligned} &\text{when} \quad t = 0, \; y(t) - y^* = y(0) - y^* \\ &\frac{d(y(0) - y^*)}{dt} = \frac{dy(0)}{dt} \end{aligned}\right\} \tag{B4}$$

The solution of equation (B3) for initial conditions (B4) can be obtained by standard methods and is as follows:

$$y-y^* = -\sum_{k=1}^{\infty} Da_k \left\{\sin\left(\frac{k\pi}{\tau}\, t-\varphi_i\right) - (-1)^k \sin\left[\frac{k\pi}{\tau}\,(t-\tau)-\varphi_i\right]\right\}$$

$$-\sum_{k=1}^{\infty} \frac{Da_k \frac{k\pi}{\tau\omega_n}}{\sqrt{1-\zeta^2}} \left\{(-1)^k\, e^{-\zeta\omega_n(t-\tau)} \sin\left[\omega_n\sqrt{1-\zeta^2}(t-\tau)-\varphi_j\right] -\right.$$

$$\left. e^{-\zeta\omega_n} \sin\left[\omega_n\sqrt{1-\zeta^2}\,t-\varphi_j\right]\right\} + \left[\frac{\frac{dy(0)}{dt} + \zeta\omega_n(y(0) - y^*)}{\omega_n\sqrt{1-\zeta^2}}\right] e^{-\zeta\omega_n t} \sin \omega_n\sqrt{1-\zeta^2}\,t +$$

$$(y(0) - y^*)\, e^{-\zeta\omega_n t} \cos \omega_n \sqrt{1-\zeta^2}\, t \qquad \text{(B5)}$$

where

$$\frac{1}{D} = \sqrt{\left[1 - \left(\frac{k\pi}{\tau\omega_n}\right)^2\right]^2 + 4\zeta^2\left(\frac{k\pi}{\tau\omega_n}\right)^2} \qquad \text{(B6)}$$

$$\varphi_j = \tan^{-1} \frac{2\zeta\sqrt{1-\zeta^2}}{\left[1 - \zeta^2 - \left(\frac{k\pi}{\tau\omega_n}\right)^2\right]}$$

$$\varphi_i = \tan^{-1} \frac{\frac{k\pi}{\tau\omega_n}\, 2\zeta}{\left[1 - \left(\frac{k\pi}{\tau\omega_n}\right)^2\right]}$$

(note: any function of $t - \tau \equiv 0$ for $t < \tau$)

The solution of equation (B3) given by equation (B5) may be separated into three parts; that is,

$$y - y^* = (y - y^*)_p + (y - y^*)_q + (y - y^*)_r \qquad \text{(B7)}$$

where

$$(y - y^*)_p = -\sum_{k=1}^{\infty} Da_k \left\{\sin\left(\frac{k\pi}{\tau}\, t - \varphi_i\right) - (-1)^k \sin\left[\frac{k\pi}{\tau}\,(t-\tau) - \varphi_i\right]\right\} \qquad \text{(B8)}$$

$$(y-y^*)_q = -\sum_{k=1}^{\infty} \frac{Da_k \frac{k\pi}{\tau\omega_n}}{\sqrt{1-\zeta^2}} \left\{(-1)^k e^{-\zeta\omega_n(t-\tau)} \sin\left[\omega_n\sqrt{1-\zeta^2}\,(t-\tau) - \varphi_j\right] - e^{-\zeta\omega_n t} \sin\left[\omega_n\sqrt{1-\zeta^2}\,t - \varphi_j\right]\right\}$$

(note: any function of $t - \tau \equiv 0$ for $t < \tau$)

and

$$(y - y^*)_r = \frac{\frac{dy(0)}{dt} + \zeta\omega_n(y(0) - y^*)}{\omega_n\sqrt{1 - \zeta^2}} e^{-\zeta\omega_n t} \sin \omega_n\sqrt{1 - \zeta^2}\, t + (y(0) - y^*)\, e^{-\zeta\omega_n t} \cos \omega_n\sqrt{1 - \zeta^2}\, t \qquad \text{(B9)}$$

The term $(y - y^*)_p$ represents the forced motion of the blade with frequency components $k\pi/\tau$, and $(y - y^*)_q$ and $(y - y^*)_r$ represent the transient motion of the blade with frequency $\omega_n\sqrt{1 - \zeta^2}$.

For the investigation reported in the body of the report, the problem was to approximate $F(t)$ from the strain-gage measurement of $y(t)$. Figure 8 shows examples of strain-gage records obtained initially. These records show the transient motions of the blade to be larger than the forced motion. At some compressor speeds the transient motions resulted in stresses sufficiently large to fatigue the web sections. In order to reduce these transient motions, a light grease was packed around the web sections of the blade as shown in figure 3. Examples of strain-gage signals obtained with the grease added are shown in figure 9. As can be seen from the figures, the damping was sufficient to nearly eliminate the transient motion between encounters with the stall zones, so that the initial conditions as a blade entered a stall zone were nearly such that $y = y^*$ and $dy/dt \cong 0$, and, consequently, $(y - y^*)_r = 0$.

Inasmuch as the additional damping had reduced the transient motion somewhat, it appeared that $F(t)$ could be determined with sufficient accuracy by filtering the transient component of the blade motion $(y - y^*)_q$ from the strain-gage signal. This filtering was accomplished by use of an electronic filter set to attenuate frequencies above 250

cps at a rate of 18 decibels per octave. Examples of filtered signals are shown in figure 10, which indicated that the transient frequencies were virtually eliminated. The wave form of the strain-gage records shown in figure 10 are approximately the wave form of the forced motion, $(y - y^*)_p$. Comparison of expressions (B8) and (B9) shows that $(y - y^*)_p$ is equal to $F(t) - F^*$ except for the magnification factor D and the phase shift φ_i.

The magnification factor D and the phase shift φ_i depend on the damping term ζ and the term $k\pi/\tau\omega_n$. As stated in the body of the report, the stall frequency was 51 cps and figure 7 shows τ to be approximately 0.01 second; then,

$$\frac{k\pi}{\tau\omega_n} \cong \frac{K50}{f_n}$$

The values of the magnification factor D and the phase shift φ_i for $k = 1, 2, 3, 4,$ and 5 for each of the four stator blades and four inlet guide vanes used in the investigation are given in table II. The damping ζ was estimated from the data. This table shows that in most cases the phase shift and magnification factor were sufficiently small so that the wave form of the forcing function $F(t) - F^*$ is satisfactorily approximated by $(y - y^*)_p$ for its fundamental and first four harmonics. Higher harmonics for which the magnification factor would be farther from unity and the phase shift larger than shown in the table were attenuated by the filter.

APPENDIX C

CALCULATION OF STEADY-STATE BLADE FORCES

The steady-state force was calculated based upon the velocity diagram considerations given in reference 8, where the axial velocity is assumed to remain constant throughout the stage. Thus the axial and tangential force components normal to the mean resultant velocity in pounds per blade become:

$$F_a = \frac{A}{gn} \rho V_{u,m} \Delta V_u \tag{C1}$$

$$F_u = \frac{A}{gn} \rho V_a \Delta V_u \tag{C2}$$

The total steady-state force for a guide vane using the vector diagram of figure 1 and combining equations (C1) and (C2) is:

$$F_o = \frac{w^2 \tan \alpha_{gv}}{gnA\rho} \sqrt{1 + \frac{\tan^2 \alpha_{gv}}{4}} \tag{C3}$$

For the circular-arc guide vanes the chord line is coincident with the mean velocity vector so that the force determined from equation (C3) is also the steady-state force normal to the chord.

In considering the steady-state forces on the stators, it appears most expedient to consider initially the component forces and to combine these later in the numerical work. Equations (C1) and (C2) utilizing the vector diagram in figure 1 are

$$F_a = \frac{wU}{2gn} \left(\frac{UA\rho}{w} - 2 \tan \alpha_s \right) \tag{C4}$$

$$F_u = \frac{w^2}{gnA\rho} \left(\frac{UA\rho}{w} - \tan \alpha_s \right) \tag{C5}$$

Since the stator blades were set at $27\frac{1}{2}^\circ$ with respect to the axis of the compressor, the steady-state force normal to the chord is

$$F_o = F_a \sin 27\tfrac{1}{2}^\circ + F_u \cos 27\tfrac{1}{2}^\circ \tag{C6}$$

The results of the numerical calculation are shown in figure 5 for the following conditions:

A, sq ft	0.203
$\alpha_{gv} = \alpha_s$, deg	$22\frac{1}{2}$
g, ft/sec^2	32.2
n for guide vanes	38
n for stators	32
U, ft/sec	580

REFERENCES

1. Huppert, Merle C., Johnson, Donald F., and Costilow, Eleanor L.: Preliminary Investigation of Compressor Blade Vibration Excited by Rotating Stall. NACA RM E52J15, 1952.

2. Huppert, Merle C.: Preliminary Investigation of Flow Fluctuations During Surge and Blade Row Stall in Axial-Flow Compressors. NACA RM E52E28, 1952.

3. Huppert, Merle C., Costilow, Eleanor L., and Budinger, Ray E.: Investigation of a 10-Stage, Axial-Flow Research Compressor. III - Investigation of Rotating Stall, Blade Vibration, and Surge at Low and Intermediate Compressor Speeds. NACA RM E53C19, 1953.

4. Huppert, Merle C., Calvert, Howard F., and Meyer, André J.: Experimental Investigation of Rotating Stall and Blade Vibration in the Axial-Flow Compressor of a Turbojet Engine. NACA RM E54A08, 1954.

5. Hanson, M. P., Meyer, A. J., Jr., and Manson, S. S.: A Method of Evaluating Loose-Blade Mounting as a Means of Suppressing Turbine and Compressor Blade Vibration. Proc. Soc. Exp. Stress Analysis, vol. 10, no. 2, Nov. 1952, pp. 103-116.

6. Pearson, H.: The Aerodynamics of Compressor Blade Vibration. The Engineer, Oct. 9, 1953, pp. 473-476.

7. Ossofsky, Eli: Constant Temperature Operation of the Hot-Wire Anemometer at High Frequency. Rev. Sci. Instr., vol. 19, no. 12, Dec. 1948, pp. 881-889.

8. Vincent, E. T.: The Theory and Design of Gas Turbines and Jet Engines. First ed., McGraw-Hill Book Co., Inc., 1950, pp. 330-331.

TABLE I. - NATURAL BLADE FREQUENCIES

Blade number	Natural frequency, cps	Web thickness, in.
Guide vane		
1	880	0.125
2	650	.094
3	500	.078
4	375	.062
Stator		
1	900	0.125
2	640	.094
3	505	.078
4	410	.062

TABLE II. - BLADE PARAMETERS

Blade number	ζ (with grease)	D				φ_i, deg			
		k→ / 2	3	4	5	k→ / 2	3	4	5
Stator									
1	0.3	1.010	1.024	1.042	1.066	3.9	5.9	8.0	10.2
2	.4	1.016	1.038	1.068	1.107	7.4	11.2	15.5	20.2
3	.5	1.019	1.052	1.073	1.107	11.6	18.4	25.2	33.3
4	.7	1.000	.994	.978	.943	20.0	30.6	41.9	53.6
Guide vane									
1	0.3	1.011	1.025	1.043	1.070	3.9	6.0	8.1	10.5
2	.4	1.016	1.037	1.065	1.100	7.2	11.0	15.2	19.9
3	.5	1.019	1.044	1.074	1.109	11.7	18.3	25.5	33.7
4	.7	1.000	.992	.967	.914	2.18	33.6	46.1	59.1

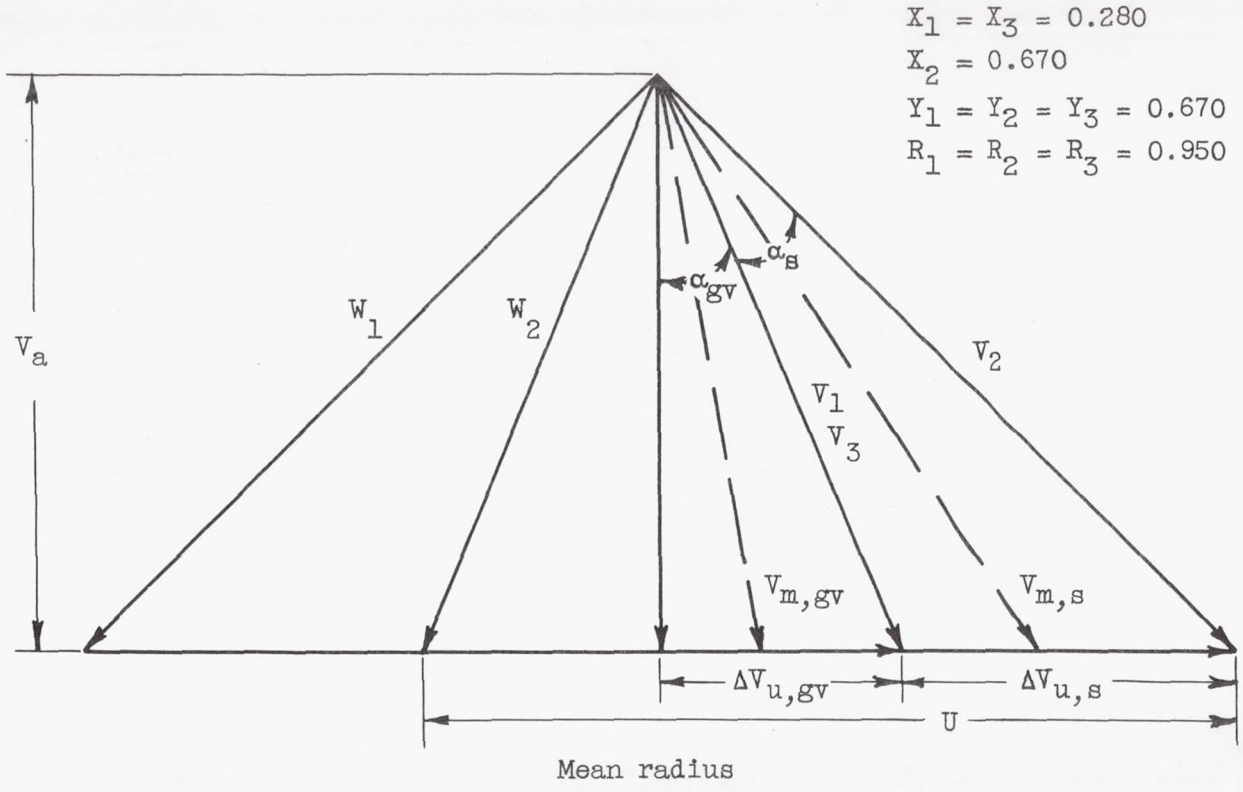

Figure 1. - Vector velocity diagrams for single-stage axial-flow compressors at 0.9 hub-tip ratio stage.

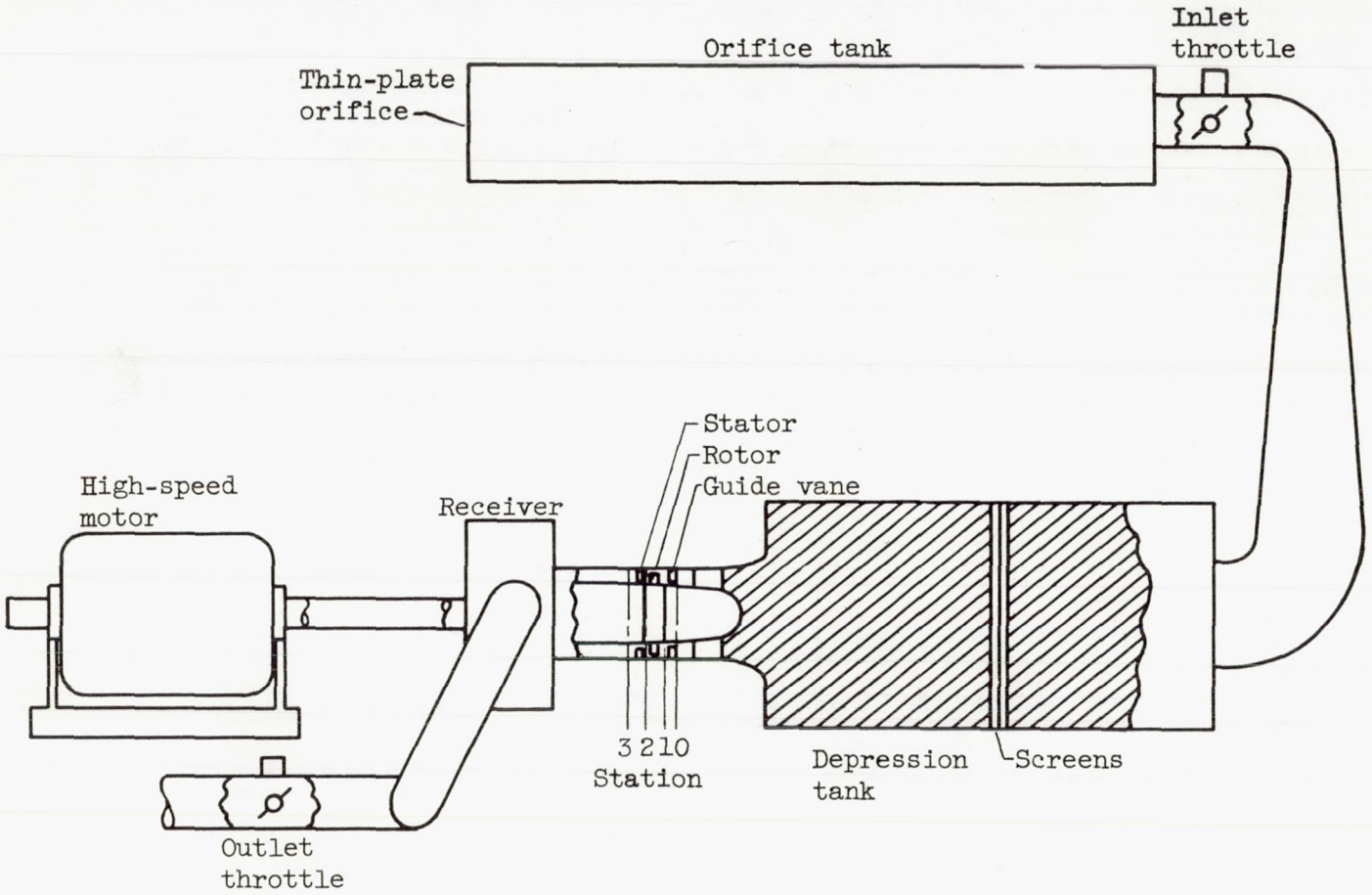

Figure 2. - Schematic diagram of compressor installation.

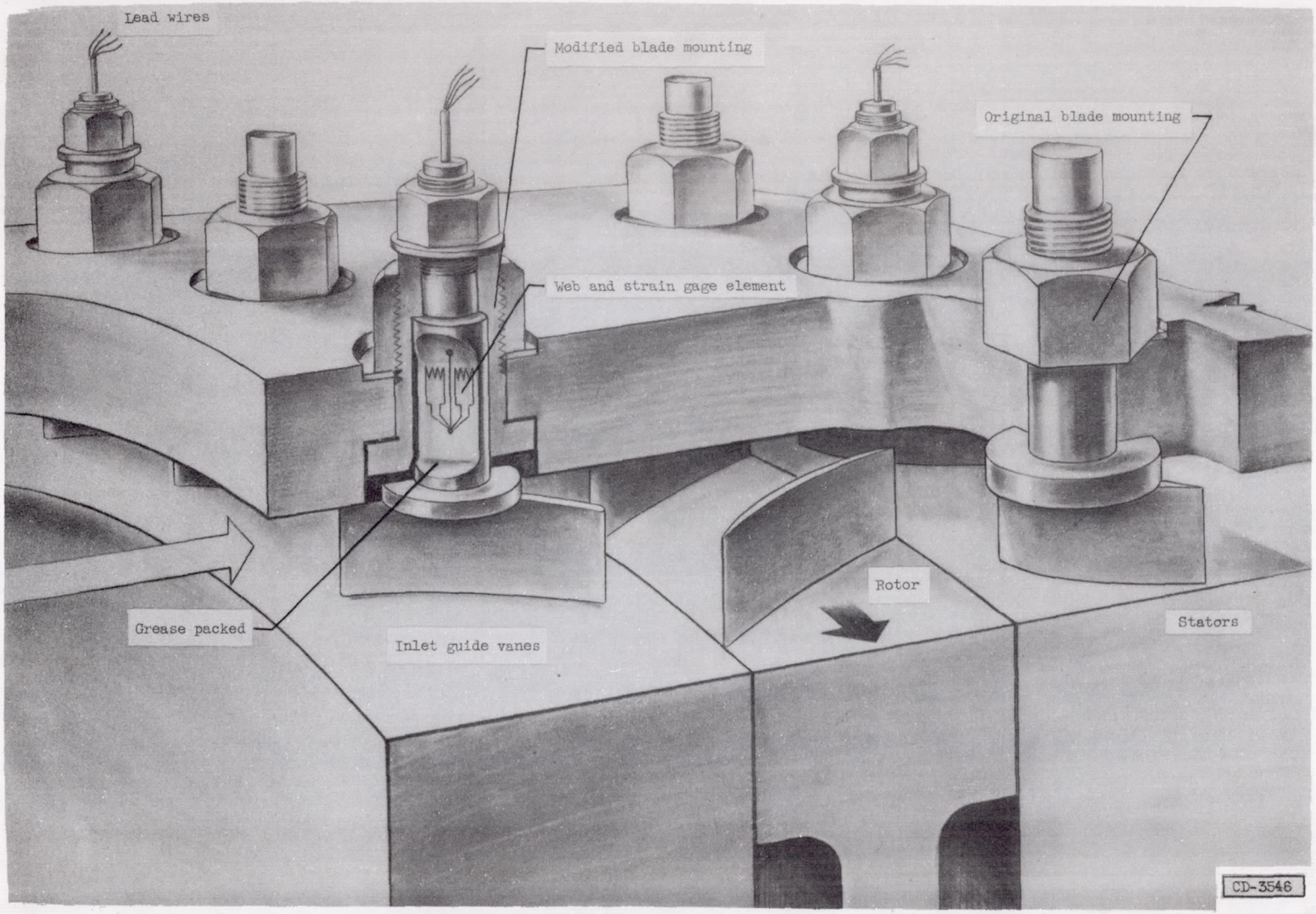

Figure 3. - Compressor and blade assembly.

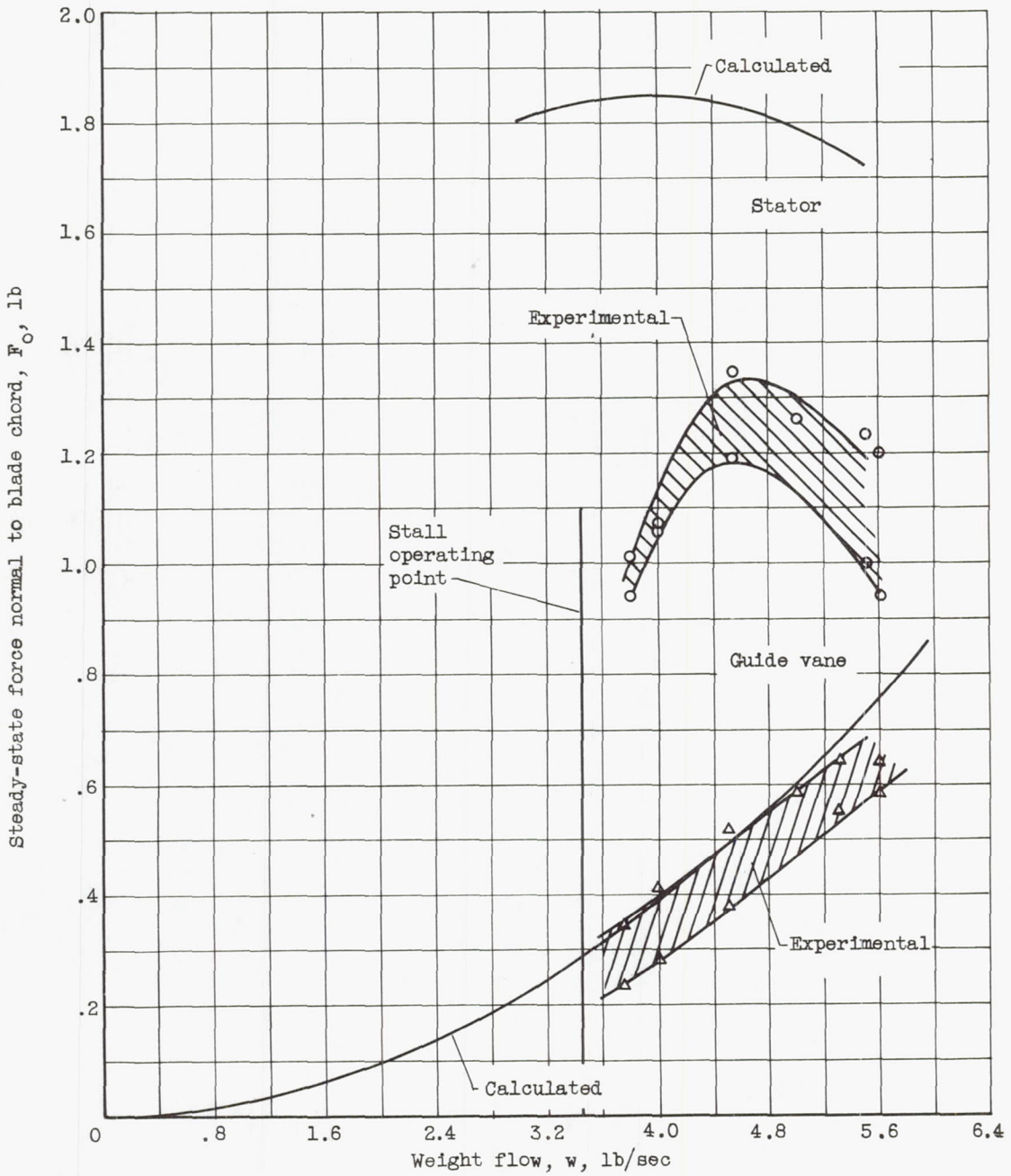

Figure 4. - Steady-state force normal to blade chord as a function of weight flow for guide vanes and stators. Corrected engine speed, $N/\sqrt{\theta}$, 167 rps.

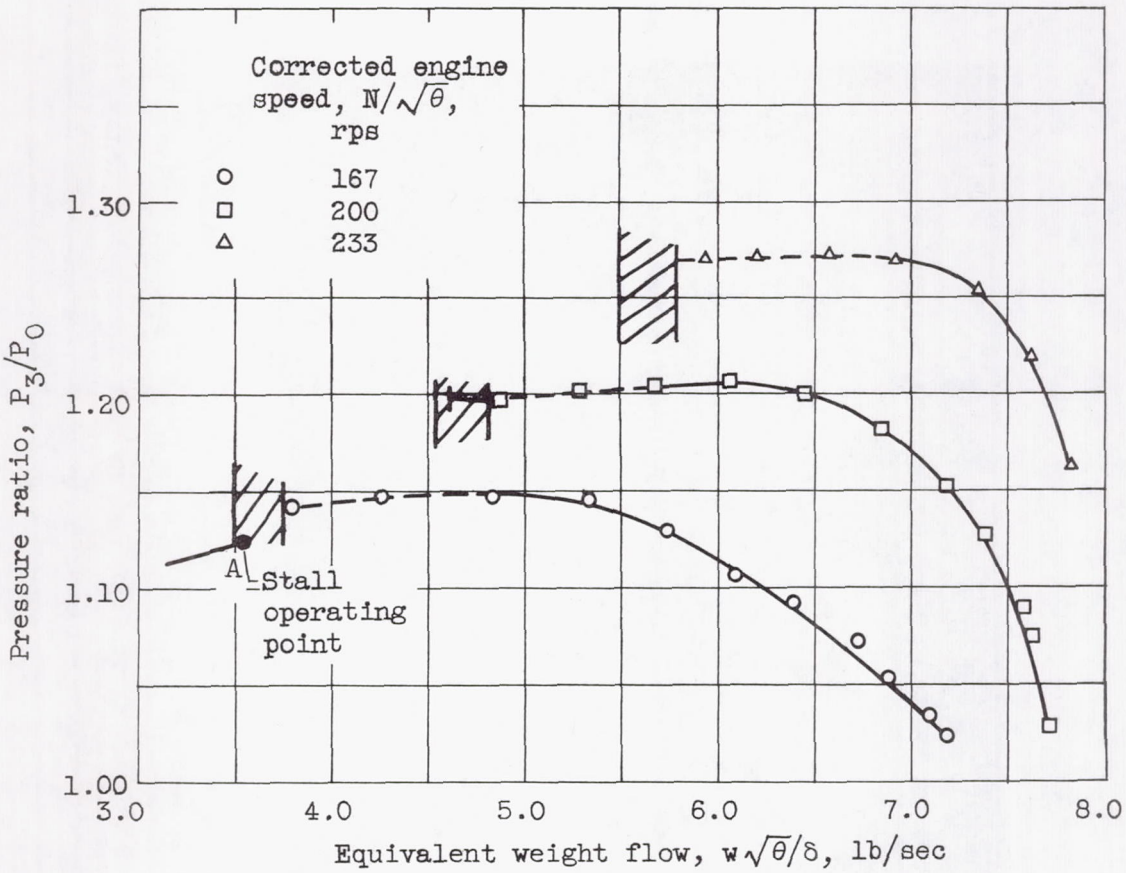

Figure 5. - Over-all performance of single-stage compressor with hub-tip ratio of 0.9.

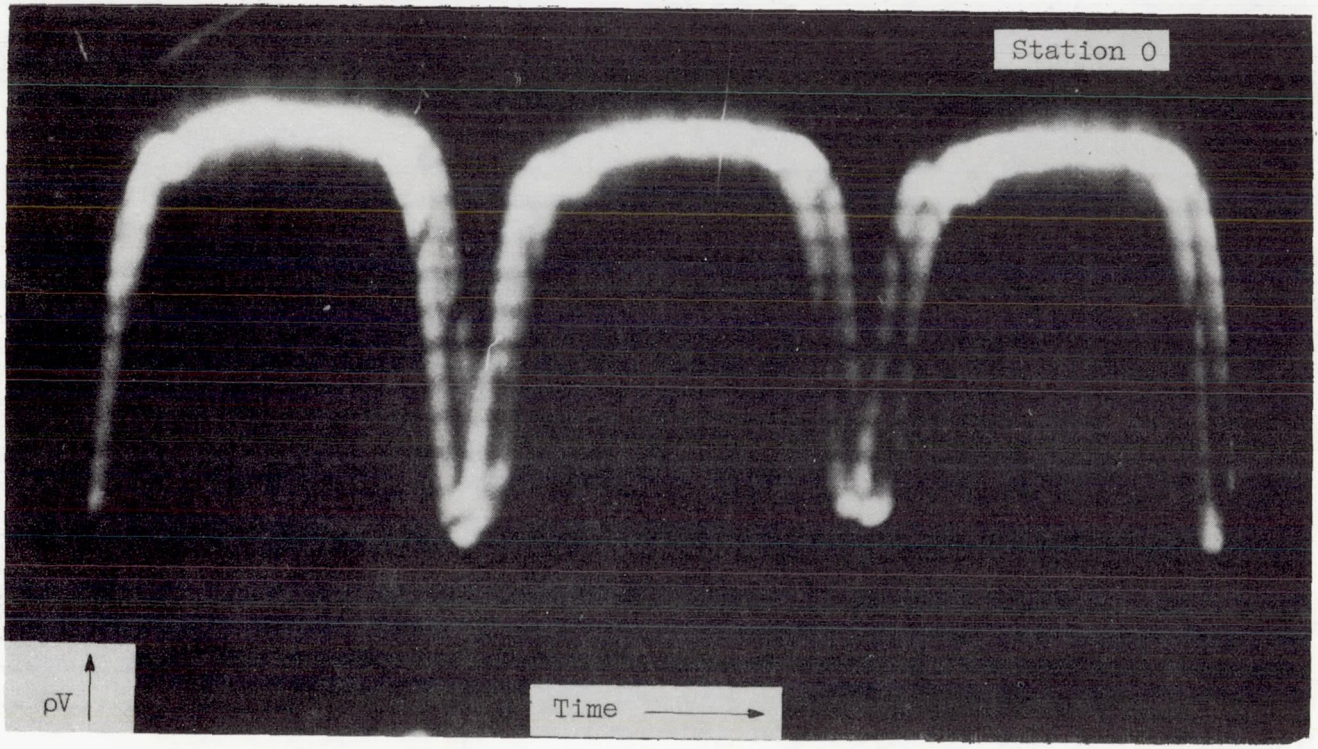

Figure 6. - Oscillogram of rotating stall at point A of figure 3. Corrected engine speed $N/\sqrt{\theta}$, 167 rps; equivalent weight flow, $w\sqrt{\theta}/\delta$, 3.55 pounds per second; frequency, f_s, 51 cps.

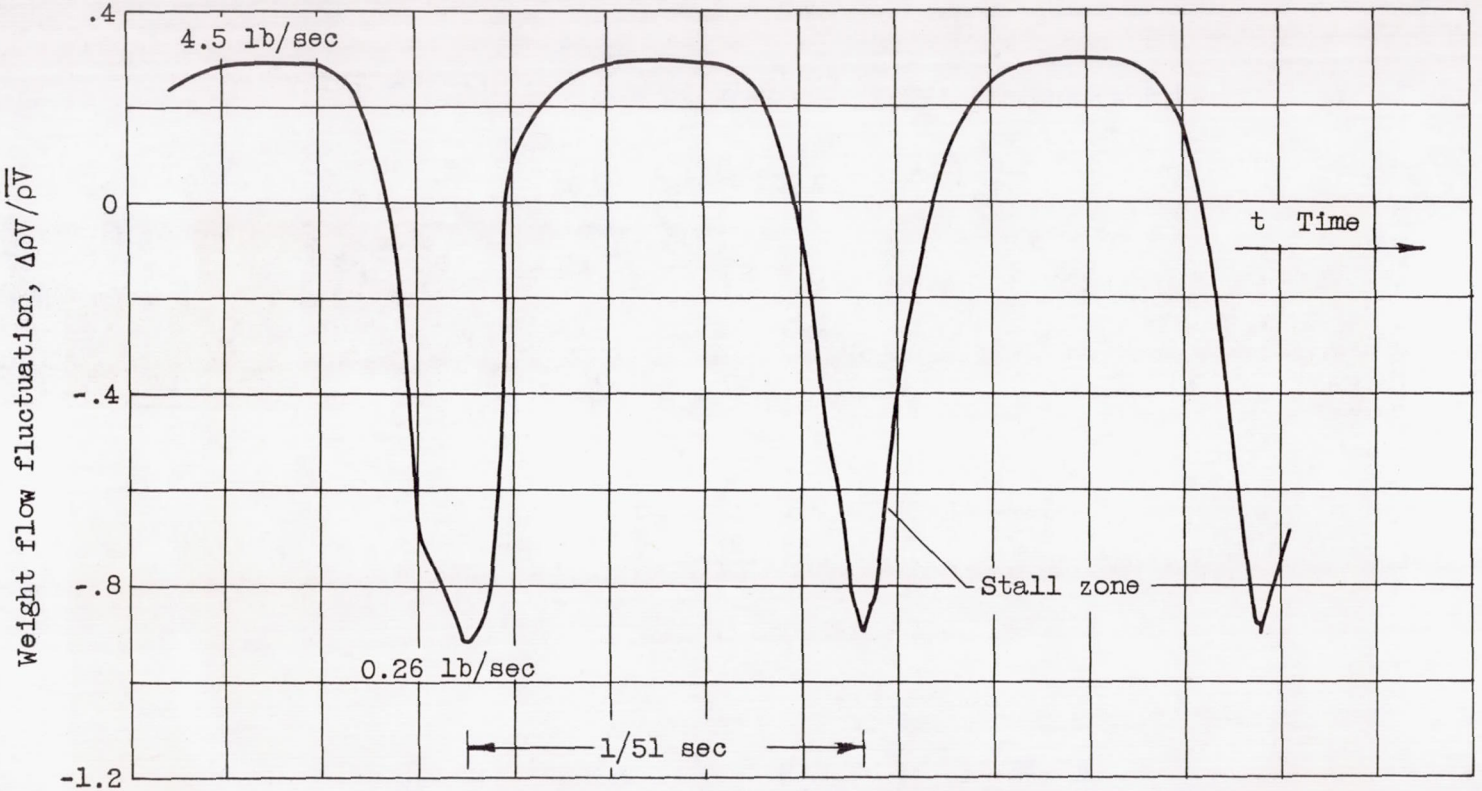

Figure 7. - Variation of weight flow in front of guide vane due to rotating stall.

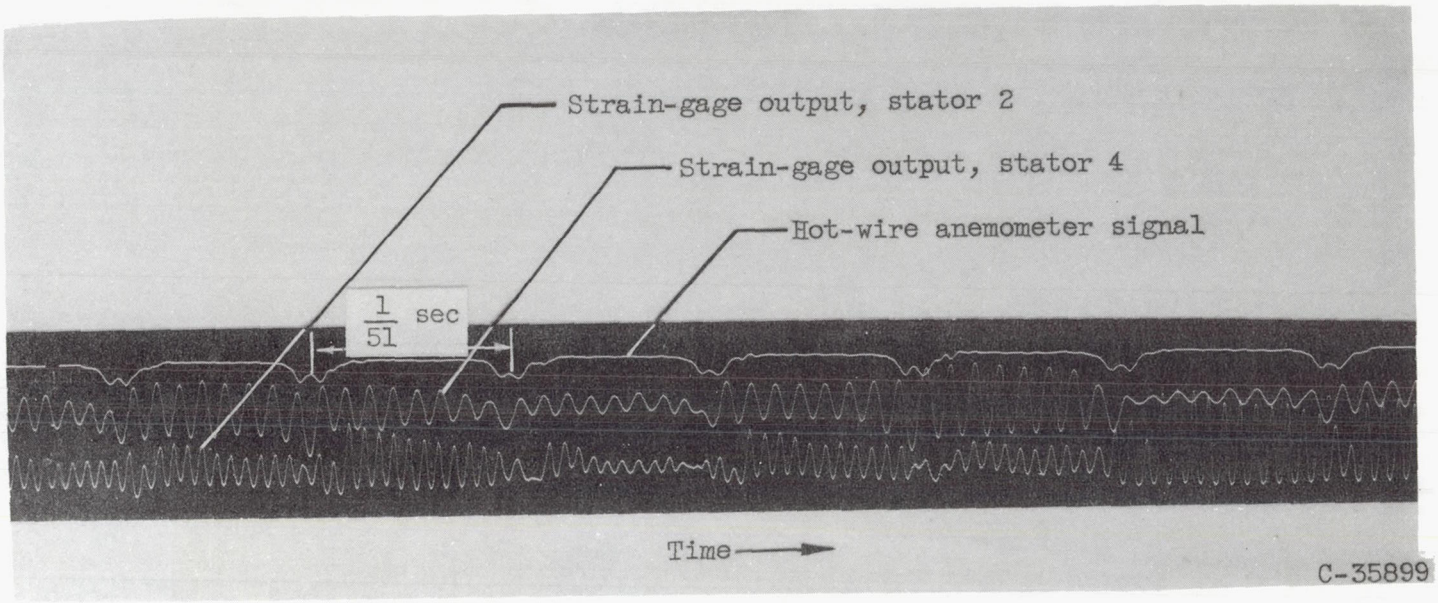

Figure 8. - Blade response with no additional viscous damping.

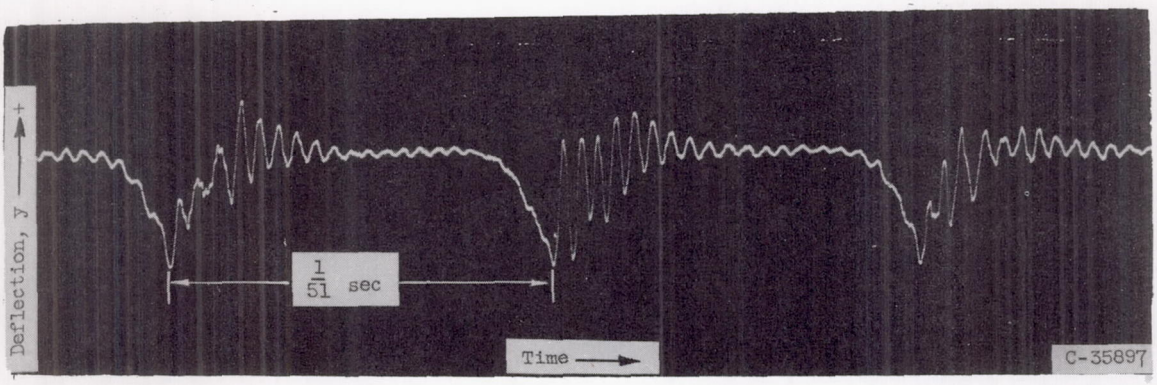

(a) Number 1 guide vane; natural blade frequency, f_n, 880 cps.

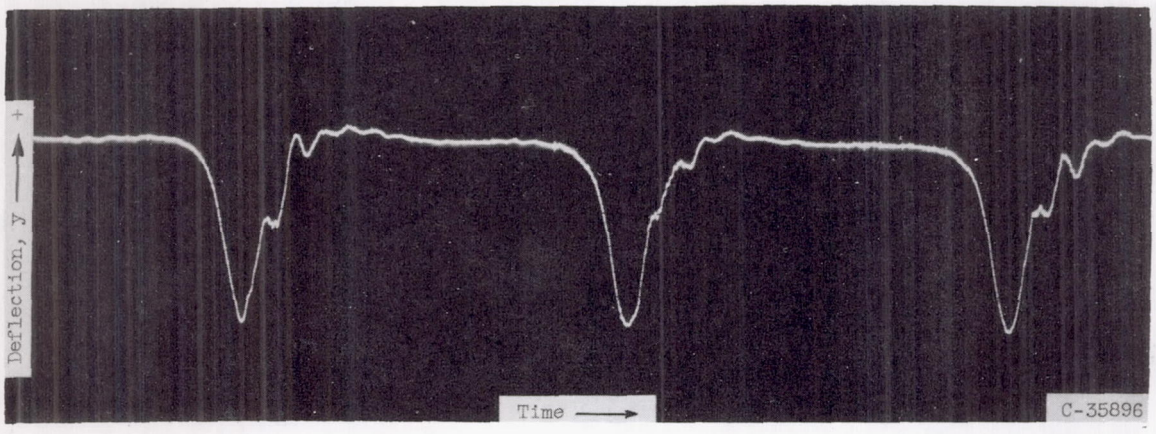

(b) Number 4 guide vane; natural blade frequency, f_n, 375 cps.

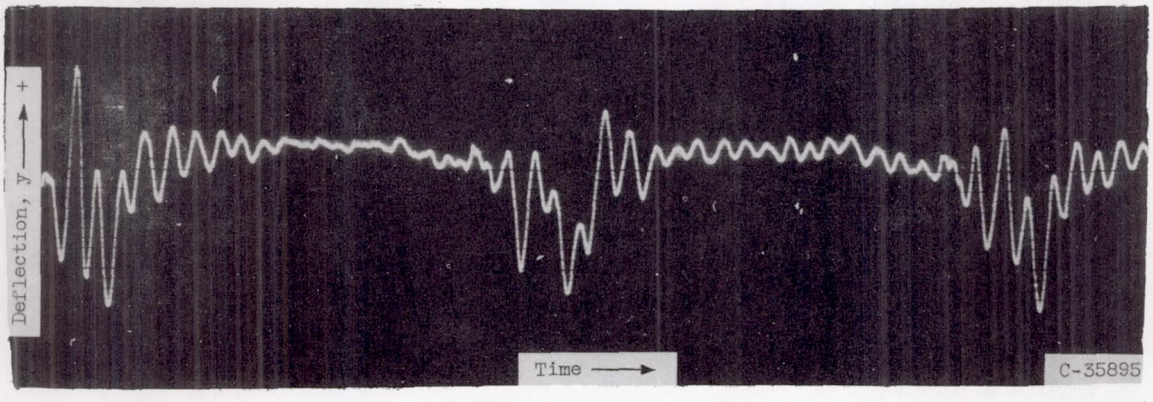

(c) Number 1 stator; natural blade frequency, f_n, 900 cps.

Figure 9. - Blade deflection oscillograms during rotating stall. Corrected engine speed, $N/\sqrt{\theta}$, 167 rps.

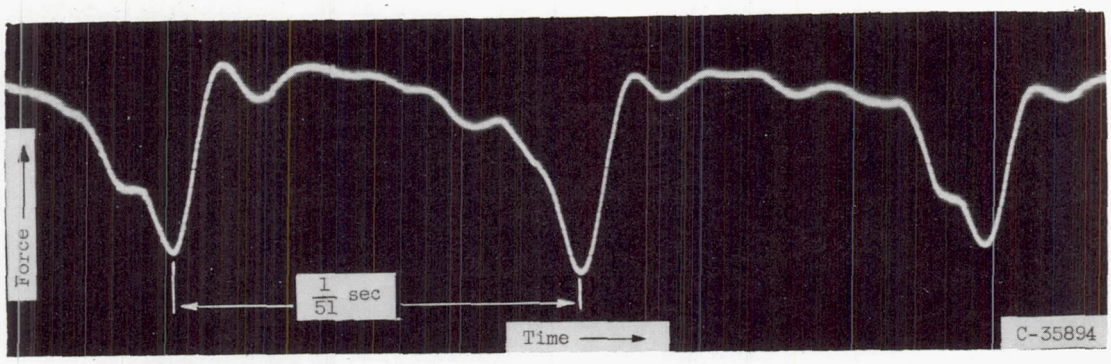

(a) Number 1 stator; natural blade frequency, f_n, 900 cps.

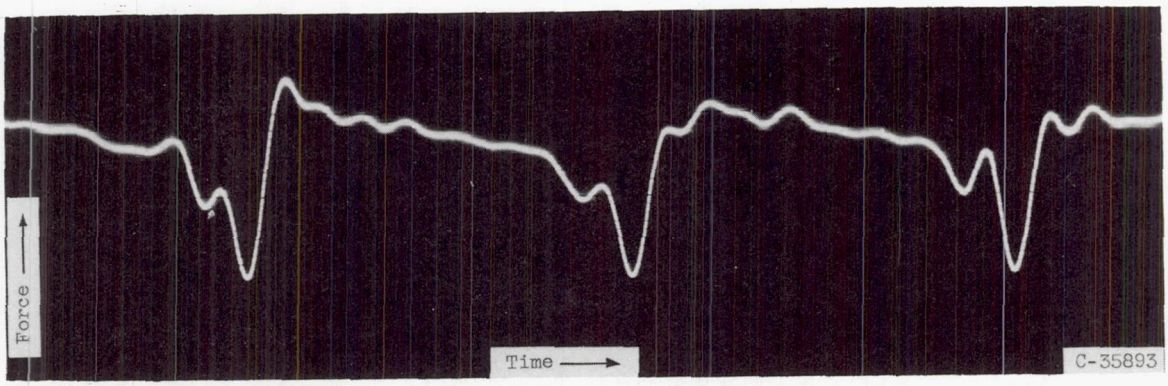

(b) Number 4 stator; natural blade frequency, f_n, 410 cps.

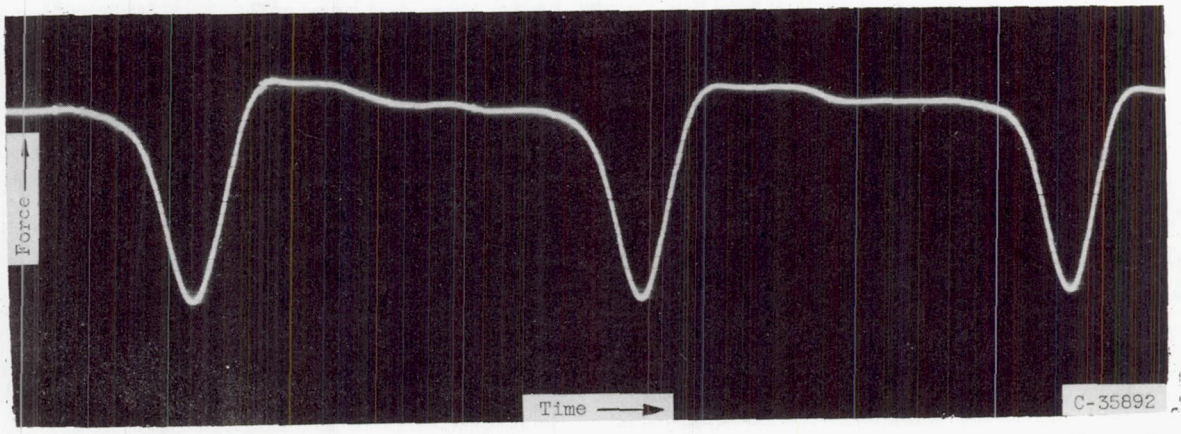

(c) Number 4 guide vane; natural blade frequency, f_n, 375 cps.

Figure 10. - Blade forcing function oscillograms during rotating stall. Corrected engine speed, $N/\sqrt{\theta}$, 167 rps.

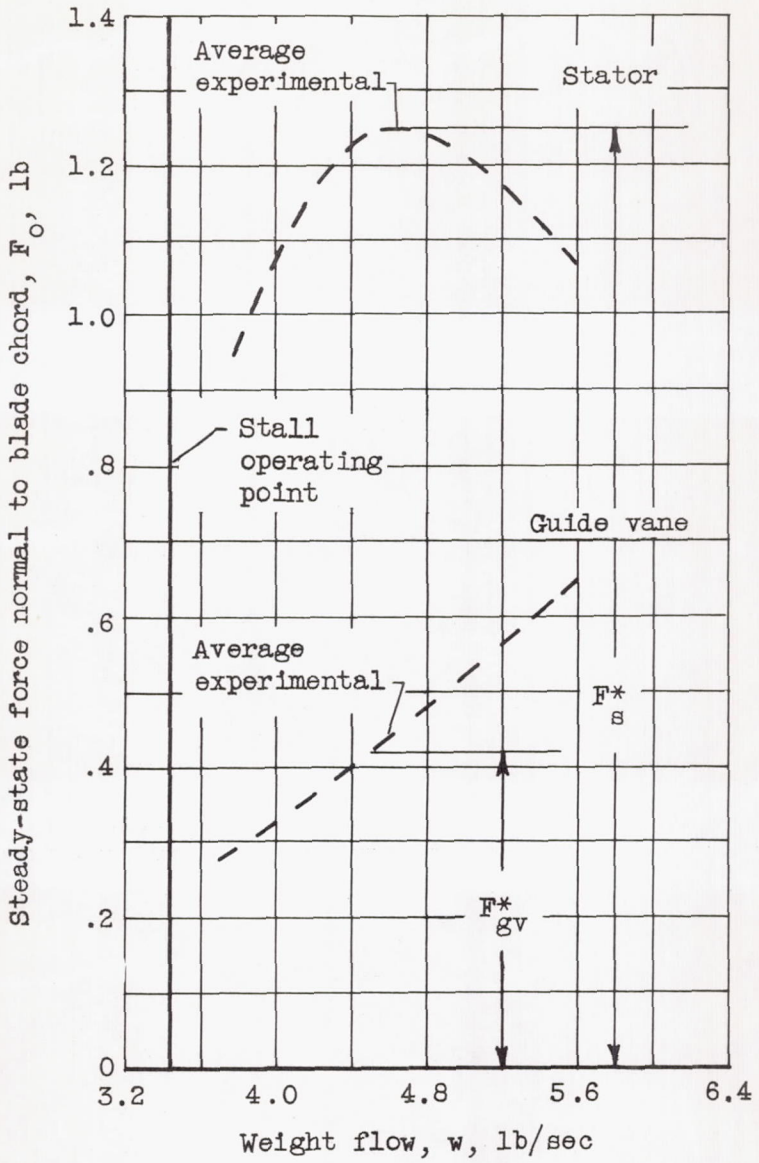

Figure 11. - Steady-state force normalizing values.